


Article

Multisensor RFS Filters for Unknown and Changing Detection Probability

Zhiguo Zhang ¹, Qing Li ² and Jinping Sun ^{1,*} ¹ Electronics & Information Engineering, Beihang University, Beijing 100191, China² Department of Engineering, University of Cambridge, Cambridge CB12PZ, UK

* Correspondence: sunjinping@buaa.edu.cn; Tel.: +86-010-82317240

Received: 16 May 2019; Accepted: 28 June 2019; Published: 30 June 2019



Abstract: The detection probability is an important parameter in multisensor multitarget tracking. The existing multisensor multi-Bernoulli (MS-MeMber) filter and multisensor cardinalized probability hypothesis density (MS-CPHD) filter require that detection probability is a priori. However, in reality, the value of the detection probability is constantly changing due to the influence of sensors, targets, and other environmental characteristics. Therefore, to alleviate the performance deterioration caused by the mismatch of the detection probability, this paper applies the inverse gamma Gaussian mixture (IGGM) distribution to both the MS-MeMber filter and the MS-CPHD filter. Specifically, the feature used for detection is assumed to obey the inverse gamma distribution and is statistically independent of the target's spatial position. The feature is then integrated into the target state to iteratively estimate the target detection probability as well as the motion state. The experimental results demonstrate that the proposed methods can achieve a better filtering performance in scenarios with unknown and changing detection probability. It is also shown that the distribution of the sensors has a vital influence on the filtering accuracy, and the filters perform better when sensors are dispersed in the monitoring area.

Keywords: multisensor multi-Bernoulli filter; multisensor cardinalized probability hypothesis density filter; detection probability; inverse gamma Gaussian mixture

1. Introduction

The objective of multitarget tracking is to jointly estimate the number and state of multiple targets from sensor observations. Recently, the tracking algorithm based on random finite set (RFS) has gained increasing attention in the field of multitarget tracking [1–3]. Unlike traditional multitarget tracking algorithms, such as multiple hypotheses tracking (MHT) [4] and joint probabilistic data association (JPDA) [5], this method directly avoids the data association step. Specifically, by treating target states and sensor measurements as RFSs, the target tracking problem is transformed into a set-valued estimation problem under the Bayesian framework. On the basis of the finite set statistics (FISST) [6], a probability hypothesis density (PHD) filter has been proposed in [7]. The PHD filter uses the moment approximation and propagates the first-order moment of the multitarget probability density, which is assumed to be Poisson-distributed. However, the cardinality variance estimated by the PHD filter grows with the number of the targets. As an improvement to the PHD filter, the cardinalized PHD (CPHD) filter [8] jointly propagates the first-order moment and the cardinality distribution. Unlike the above RFS filters based on the moment approximation, the multitarget multi-Bernoulli (MeMber) filter proposed in [6] directly approximates the multitarget posterior with multi-Bernoulli components, and thus more density information is preserved in the Bayesian recursion. However, the first-order Taylor linear approximation in the updating process introduces a cardinality estimation bias [9], and thus a cardinalized MeMber (CBMeMber) filter is proposed in [10] to eliminate this bias. The limit of

the multi-Bernoulli filter is that it can only accommodate target states. Therefore, the δ -generalized labeled multi-Bernoulli (δ -GLMB) filter which can output target tracks has been developed [11], and two approximations of the δ -GLMB filter, labeled the multi-Bernoulli (LMB) filter and the marginalized δ -GLMB filter, have been designed to reduce the computational cost [12,13]. Nevertheless, when the track estimation is not needed, the multi-Bernoulli filter and the CPHD/PHD filters have been shown to be more efficient compared with the labeled RFS filters; thus, they have been widely used [14–16].

A number of RFS tracking methods have also been studied in the multisensor field [17–22]. Mahler [17] derived a generalized PHD (G-PHD) filter for the case of two sensors, and Delande et al. [18] extended it to scenarios with an arbitrary number of sensors. To avoid the combinatorial computational complexity of the G-PHD filter, the iterated corrector PHD (IC-PHD) filter was proposed in [19]. The parallel-combination approximate multisensory (PCAM) PHD filter [20] is a theoretical approximation of multisensor PHD filters and is independent of the sensor order. In [21], the multisensor CPHD (MS-CPHD) filter was introduced, and the multisensor MeMber (MS-MeMber) filter was proposed in [22]. Based on the labeled RFS, the centralized multisensor δ -GLMB (MS- δ -GLMB) with extended association maps was introduced in [23].

The detection probability is usually considered as a known parameter in general tracking algorithms. Whereas in real scenarios, the detection probability is affected by sensors, targets, the environment, and the features used for detection [24]. For instance, Mahler et al. [25] proposed CPHD/PHD filters that can accommodate parameter mismatch in the clutter rate and detection profile in which the detection probability is obtained by the Beta Gaussian mixture (BGM) model. Subsequently, a multitarget multi-Bernoulli filter [26,27] was proposed to adaptively learn the nonhomogeneous clutter intensity and detection probability. Meanwhile, a multitarget tracker based on the labeled RFS was proposed in [28], which can estimate the clutter rate and detection profile. All these filters assume that the detection probability is Beta-distributed and calculate the detection probability through the accumulation of observation effects in the BGM model. However, the filtering performance deteriorates when the detection probability is low, and poor model initialization parameters can adversely affect the filtering performance. For this reason, the inverse gamma Gaussian mixture (IGGM) model is used in CPHD/PHD filters [29]. Specifically, the feature used for detection is an inverse gamma distribution, and by combining the feature into the target motion state, the performance loss caused by the mismatch of the detection probability parameters is reduced.

In the field of multisensor and multitarget tracking, the MS-CPHD filter and MS-MeMber filter are two important methods, and the ways they are generalized to handle scenarios with an unknown and time varying detection of probability are similar. Therefore, in this paper, we propose IGGM-MS-CPHD/MeMber filters for the unknown and varying detection probability case. Initially, we incorporated the detection feature into the target motion state. On the basis of the augmented state, the IGGM model was applied to both the MS-CPHD filter and the MS-MeMber filter to iteratively estimate the detection probability and motion parameters. Then the estimated detection probability was updated to the next step for further filtering. The simulation results show that compared to GM-based MS-CPHD/MeMber filters, the proposed filters achieve a better performance when the detection probability is unknown and dynamically changing and when sensors are dispersed in the observation area.

This paper is organized as follows: Section 2 gives a review of the MS-CPHD/MeMber filters and the IGGM model, the proposed IGGM-MS-CPHD/MeMber filters are derived in Section 3, the simulation results are presented in Section 4, and the conclusions are given in Section 5.

2. Background

In this section, we present the basic materials for the MS-CPHD/MeMber filters and the IGGM model.

2.1. Multisensor Measurement Partitioning

Measurement partitioning means that the measurement set is divided into a finite number of mutually disjoint subsets. The MS-CPHD/MeMber filters have high computational complexity since all measurement partitioning forms are required for calculating the accurate solution. To improve the efficiency, Nannuru et al. [21] proposed a greedy measurement partitioning algorithm that obtains a finite number of partitioning hypotheses to derive an approximate solution of the MS-CPHD filter. Subsequently, Sančan et al. applied this partitioning algorithm to the MS-MeMber filter in [22]. The objective of the greedy measurement partitioning algorithm is to recombine the multisensor observations and obtain several measurement partitioning hypotheses. Assume that $\mathbf{Z}_k^{1:s} = \{\mathbf{Z}_k^1, \mathbf{Z}_k^2, \dots, \mathbf{Z}_k^s\}$ is the observation set generated by all the s sensors at time k , where \mathbf{Z}_k^j is the measurement set generated by the j th sensor. Then by using the greedy measurement partitioning algorithm, $\mathbf{Z}_k^{1:s}$ can be reconstructed as $\mathbf{Z}_k^{1:s} = \mathbf{P} = \{\mathbf{W}_{1:s}^1, \mathbf{W}_{1:s}^2, \dots, \mathbf{W}_{1:s}^{|\mathbf{P}|-1}, \mathbf{V}\}$, where \mathbf{P} is the measurement partitioning hypothesis. $\mathbf{W}_{1:s}^j$ denotes the measurements generated by target j from all sensors at time k , \mathbf{V} is the clutter measurements from all sensors, and the divided parts follow Equations (1)–(3):

$$\mathbf{W}_{1:s}^i \cap \mathbf{W}_{1:s}^j = \emptyset, 1 \leq i \neq j \leq |\mathbf{P}|-1, \tag{1}$$

$$\mathbf{W}_{1:s}^i \cap \mathbf{V} = \emptyset, 1 \leq i \leq |\mathbf{P}|-1, \tag{2}$$

$$\mathbf{W}_{1:s}^1 \cup \mathbf{W}_{1:s}^2 \cup \dots \cup \mathbf{W}_{1:s}^{|\mathbf{P}|-1} \cup \mathbf{V} = \mathbf{Z}_k^{1:s}. \tag{3}$$

Define \mathbf{Q} to be the set composed of the measurement partitioning hypothesis \mathbf{P} , $T_{\mathbf{W}_{1:s}^j} = \{(i, l) | \mathbf{z}_l^i \in \mathbf{W}_{1:s}^j\}$ is a mapping function, and \mathbf{z}_l^i is the l th measurement in the observation set generated by sensor i .

2.2. The MS-CPHD Filter

The prediction process of the MS-CPHD filter is the same as that of the single-sensor CPHD filter in [8]. Define \mathbf{x} as the state vector of the target. Assume that the first-order moment of the multitarget posterior at time $k-1$ is $D_{k-1|k-1}(\mathbf{x})$ and the cardinality distribution is $p_{k-1|k-1}(n)$, then the predicted PHD function is given by

$$D_{k|k-1}(\mathbf{x}) = \langle \rho_{sv}(\mathbf{x}) f_{k|k-1}(\mathbf{x}|\cdot), D_{k-1|k-1} \rangle + b_k(\mathbf{x}), \tag{4}$$

and the predicted cardinality distribution follows

$$p_{k|k-1}(n) = \sum_{j=0}^n p_{b,k}(n-j) \sum_{l=j}^{\infty} C_j^l p_{k-1|k-1}(l) \frac{\langle D_{k-1|k-1}, \rho_{sv} \rangle^j \langle D_{k-1|k-1}, 1 - \rho_{sv} \rangle^{l-j}}{\langle D_{k-1|k-1}, 1 \rangle^l}, \tag{5}$$

where $b_k(\mathbf{x})$ and $p_{b,k}(n-j)$ are the first-order moment and cardinality distribution of the newborn targets at time k , respectively. $f_{k|k-1}(\mathbf{x}|\cdot)$ is the transfer function. The combination coefficient follows $C_j^l = l! / (j!(l-j)!)$, and $\rho_{sv}(\mathbf{x})$ is the survival probability of the target with state \mathbf{x} at time k .

The updated PHD equation of the MS-CPHD filter is

$$\frac{D_{k|k}(\mathbf{x})}{r_{k|k-1}(\mathbf{x})} = \alpha_0 \prod_{j=1}^s q_d^j(\mathbf{x}) + \sum_{\mathbf{P} \in \mathbf{Q}} \alpha_{\mathbf{P}} \left(\sum_{j=1}^{|\mathbf{P}|-1} \rho_{\mathbf{W}_{1:s}^j}(\mathbf{x}) \right), \tag{6}$$

where

$$\alpha_0 = \frac{\sum_{\mathbf{P} \in \mathbf{Q}} \left(K_{\mathbf{P}} M^{(|\mathbf{P}|)}(\gamma) \prod_{j=1}^{|\mathbf{P}|-1} d_{\mathbf{W}_{1:s}^j} \right)}{\sum_{\mathbf{P} \in \mathbf{Q}} \left(K_{\mathbf{P}} M^{(|\mathbf{P}|-1)}(\gamma) \prod_{j=1}^{|\mathbf{P}|-1} d_{\mathbf{W}_{1:s}^j} \right)}, \tag{7}$$

$$\alpha_{\mathbf{P}} = \frac{K_{\mathbf{P}} M^{(|\mathbf{P}|-1)}(\gamma) \prod_{j=1}^{|\mathbf{P}|-1} d_{\mathbf{W}_{1:s}^j}}{\sum_{\mathbf{U} \in \mathbf{Q}} \left(K_{\mathbf{U}} M^{(|\mathbf{U}|-1)}(\gamma) \prod_{j=1}^{|\mathbf{U}|-1} d_{\mathbf{W}_{1:s}^j} \right)}, \tag{8}$$

$$\rho_{\mathbf{W}_{1:s}^j}(\mathbf{x}) = \frac{\left(\prod_{(i,l) \in T_{\mathbf{W}_{1:s}^j}} p_d^i(\mathbf{x}) g_i(\mathbf{z}_l^i | \mathbf{x}) \right) \prod_{(i,*) \notin T_{\mathbf{W}_{1:s}^j}} q_d^i(\mathbf{x})}{\int r_{k|k-1}(\mathbf{x}) \left(\prod_{(i,l) \in T_{\mathbf{W}_{1:s}^j}} p_d^i(\mathbf{x}) g_i(\mathbf{z}_l^i | \mathbf{x}) \right) \prod_{(i,*) \notin T_{\mathbf{W}_{1:s}^j}} q_d^i(\mathbf{x}) d\mathbf{x}}. \tag{9}$$

The normalized function for the predicted PHD $D_{k|k-1}(\mathbf{x})$ is $r_{k|k-1}(\mathbf{x})$. Assume $\alpha_{\mathbf{P}}$ as the weight of the measurement partitioning hypothesis \mathbf{P} in the set \mathbf{Q} , and the all-clutter partitioning hypothesis has an associated weight α_0 . $d_{\mathbf{W}_{1:s}^j}$ denotes the weight of $\mathbf{W}_{1:s}^j$ in hypothesis \mathbf{P} , and \mathbf{U} is also a measurement partitioning hypothesis. $p_d^i(\mathbf{x})$ is the detection probability of the target with state \mathbf{x} by sensor i , and $q_d^i(\mathbf{x}) = 1 - p_d^i(\mathbf{x})$. $g_i(\mathbf{z}_l^i | \mathbf{x})$ is the measurement likelihood of sensor i . The probability that the target with state \mathbf{x} is not detected by any sensor is given by $\gamma = \int r_{k|k-1}(\mathbf{x}) \prod_{j=1}^S q_d^j(\mathbf{x}) d\mathbf{x}$. $K_{\mathbf{P}} = \prod_{i=1}^S C_i^{(m_i - |\mathbf{P}|)}(0)$. $C_i^{(n)}(\cdot)$ and $M_i^{(n)}(\cdot)$ are the n th-order derivatives of the probability generating functions (PGFs) of the clutter cardinality distribution and the predicted cardinality distribution, respectively.

After the updating process, the posterior cardinality distribution is

$$p_{k|k}(n) = p_{k|k-1}(n) \frac{\sum_{\mathbf{P} \in \mathbf{Q}} \left(K_{\mathbf{P}} \frac{n!}{(n - |\mathbf{P}| + 1)!} \gamma^{n - |\mathbf{P}| + 1} \prod_{j=1}^{|\mathbf{P}|-1} d_{\mathbf{W}_{1:s}^j} \right) \mathbb{1}_{|\mathbf{P}| \leq n + 1}}{\sum_{\mathbf{P} \in \mathbf{Q}} K_{\mathbf{P}} M^{(|\mathbf{P}|-1)}(\gamma) \prod_{j=1}^{|\mathbf{P}|-1} d_{\mathbf{W}_{1:s}^j}}. \tag{10}$$

2.3. The MS-MeMber Filter

Since no observation information is required in the prediction process, the predicted density of the MS-MeMber filter is the same as that of the MeMber/CBMeMber filters [9,10]. Suppose that at time $k-1$, the multitarget density is a multi-Bernoulli of the form

$$\pi_{k-1|k-1} = \left\{ (r_{k-1|k-1}^{(i)}, p_{k-1|k-1}^{(i)}) \right\}_{i=1}^{M_{k-1|k-1}}, \tag{11}$$

where $M_{k-1|k-1}$ is the component number. Then the predicted multitarget density is also a multi-Bernoulli and is formed by the union of surviving sets $\left\{ (r_{S,k|k-1}^{(i)}, p_{S,k|k-1}^{(i)}) \right\}_{i=1}^{M_{k-1|k-1}}$ and newborn sets $\left\{ (r_{b,k}^{(i)}, p_{b,k}^{(i)}) \right\}_{i=1}^{M_{b,k}}$, i.e.,

$$\left\{ (r_{k|k-1}^{(i)}, p_{k|k-1}^{(i)}) \right\}_{i=1}^{M_{k|k-1}} = \left\{ (r_{S,k|k-1}^{(i)}, p_{S,k|k-1}^{(i)}) \right\}_{i=1}^{M_{k-1|k-1}} \cup \left\{ (r_{b,k}^{(i)}, p_{b,k}^{(i)}) \right\}_{i=1}^{M_{b,k}}, \tag{12}$$

where $r^{(i)}$ in Equation (12) is the existence probability of target i , and $p^{(i)}(\cdot)$ is the corresponding density function. The surviving multi-Bernoulli components are given by Equations (13) and (14):

$$r_{S,k|k-1}^{(i)} = r_{k-1|k-1}^{(i)} \left\langle p_{k-1|k-1}^{(i)}, \rho_{sv} \right\rangle, \tag{13}$$

$$p_{S,k|k-1}^{(i)}(\mathbf{x}) = \frac{\left\langle f_{k|k-1}(\mathbf{x}), p_{k-1|k-1}^{(i)} \rho_{sv} \right\rangle}{\left\langle p_{k-1|k-1}^{(i)}, \rho_{sv} \right\rangle}. \tag{14}$$

As the updated multitarget posterior density $\pi_{k|k}$ no longer has the original form, an approximate multi-Bernoulli distribution $\hat{\pi}_{k|k} = \bigcup_{\mathbf{P} \in \mathbf{Q}} \bigcup_{j=1}^{M_{k|k-1}} \left\{ (r_{k|k}^{(\mathbf{P},j)}, p_{k|k}^{(\mathbf{P},j)}) \right\}$ with an equal PHD function is derived in [16], where

$$r_{k|k}^{(\mathbf{P},j)} = \begin{cases} \alpha_{\mathbf{P}} \frac{r_{k|k-1}^{(j)} \left\langle p_{k|k-1}^{(j)}, \gamma \right\rangle}{1 - r_{k|k-1}^{(j)} + r_{k|k-1}^{(j)} \left\langle p_{k|k-1}^{(j)}, \gamma \right\rangle} & \mathbf{W}_{1:s}^j = \emptyset \\ \alpha_{\mathbf{P}} & \mathbf{W}_{1:s}^j \neq \emptyset \end{cases}, \tag{15}$$

$$p_{k|k}^{(\mathbf{P},j)}(\mathbf{x}) = \begin{cases} \frac{p_{k|k-1}^{(j)}(\mathbf{x}) \gamma(\mathbf{x})}{\left\langle p_{k|k-1}^{(j)}, \gamma \right\rangle} & \mathbf{W}_{1:s}^j = \emptyset \\ \frac{p_{k|k-1}^{(j)}(\mathbf{x}) f(\mathbf{W}_{1:s}^j | \mathbf{x})}{\int p_{k|k-1}^{(j)}(\mathbf{x}) f(\mathbf{W}_{1:s}^j | \mathbf{x}) d\mathbf{x}} & \mathbf{W}_{1:s}^j \neq \emptyset \end{cases}. \tag{16}$$

In Equation (16), the probability that the target with state \mathbf{x} is not detected by any sensor is given by $\gamma(\mathbf{x}) = \prod_{i=1}^s (1 - p_d^i(\mathbf{x}))$. Define $f(\mathbf{W}_{1:s}^j | \mathbf{x})$ to be the multisensor likelihood for the single target with state \mathbf{x} :

$$f(\mathbf{W}_{1:s}^j | \mathbf{x}) \triangleq \prod_{(i,l) \in T_{\mathbf{W}_{1:s}^j}} \frac{p_d^i(\mathbf{x}) g_l(\mathbf{z}_l^i | \mathbf{x})}{c(\mathbf{z}_l^i)} \prod_{(i,*) \notin T_{\mathbf{W}_{1:s}^j}} (1 - p_d^i(\mathbf{x})). \tag{17}$$

$c(\cdot)$ is the density function of the clutter. The weight of the measurement partitioning hypothesis \mathbf{P} in set \mathbf{Q} is

$$\alpha_{\mathbf{P}} \triangleq \frac{K_{\mathbf{P}} \prod_{j=1}^{M_{k|k-1}} \varphi_{\mathbf{W}_{1:s}^j}^j [1]}{\sum_{\mathbf{U} \in \mathbf{Q}} K_{\mathbf{U}} \prod_{j=1}^{M_{k|k-1}} \varphi_{\mathbf{W}_{1:s}^j}^j [1]}, \tag{18}$$

where

$$\varphi_{\mathbf{W}_{1:s}^j}^j [u] \triangleq \begin{cases} 1 - r_{k|k-1}^{(j)} + r_{k|k-1}^{(j)} \left\langle p_{k|k-1}^{(j)}, u \gamma \right\rangle & \mathbf{W}_{1:s}^j = \emptyset \\ r_{k|k-1}^{(j)} \int u(\mathbf{x}) p_{k|k-1}^{(j)}(\mathbf{x}) f(\mathbf{W}_{1:s}^j | \mathbf{x}) d\mathbf{x} & \mathbf{W}_{1:s}^j \neq \emptyset \end{cases}. \tag{19}$$

2.4. The IGGM Model

The CPHD/PHD filters for scenarios with an unknown detection probability were proposed in [18]. This method assumes that the detection probability is Beta-distributed, and the detection probability is calculated through the accumulation of observation effects. However, the filtering performance decreases significantly when the detection probability is low. In practice, the target detection probability depends on the features used for detection. For example, the gray-scale characteristics and structures of the infrared target [30] need to be considered, and, in radar detection, the signal-to-noise ratio (SNR) and the amplitude are crucial for determining the target detection probability [31–33]. Generally, these features are usually non-negative and non-Gaussian. In addition, the stronger the SNR and echo amplitude the higher the target detection probability. Therefore, the IGGM model and its analytical form

of CPHD/PHD filters were proposed in [29]. In the IGGM model, it is assumed that the single-target state \mathbf{x} contains the kinematic state $\tilde{\mathbf{x}}$ and also the feature a used for detection, i.e., $\mathbf{x} = [\tilde{\mathbf{x}}, a]^T$. Then the measurement state can be denoted as $\mathbf{z} = [\tilde{\mathbf{z}}, h]^T$, where $\tilde{\mathbf{z}}$ is the position measurement and h is the feature measurement. In a short time, rather than the target's position, the SNR and echo amplitude are mainly dependent on the radar reflection cross section (RCS) and the target's shape. Thus it can be assumed that the feature a is statistically independent of the kinematic state $\tilde{\mathbf{x}}$, and the detection probability is determined by the feature a , i.e., $p_{d,k}(\tilde{\mathbf{x}}, a) = p_{d,k}(a)$.

The probability density of the inverse gamma distribution $IG(x; u, v)$ is

$$IG(x; u, v) = \frac{v^u}{\Gamma(u)} x^{-u-1} \exp(-\frac{v}{x}), \tag{20}$$

where variable $x > 0$, shape parameter $u > 0$, and scale parameter $v > 0$. $\Gamma(\cdot)$ denotes the gamma function. The mode of the inverse gamma distribution is $v/u + 1$, and the mean value is $v/u - 1$.

Accordingly, the probability density of the gamma distribution follows

$$G(x; u, v) = \frac{v^u}{\Gamma(u)} x^{u-1} \exp(-vx), \tag{21}$$

where $x > 0$, $u > 0$, and $v > 0$. In Equation (21), the mode and mean values are $(u - 1)/v$ and u/v , respectively.

Assume that at time $k-1$, feature a obeys the inverse gamma distribution with

$$f_{k-1|k-1}(a) = IG(a; u_{k-1}, v_{k-1}), \tag{22}$$

the Markov transfer density $L_{k|k-1}(a|a')$ with feature a' is determined as follows:

$$f_{k|k-1}(a) = \int L_{k|k-1}(a|a') \cdot f_{k-1|k-1}(a') da', \tag{23}$$

$$f_{k|k-1}(a) = IG(a; u_{k|k-1}, v_{k|k-1}), \tag{24}$$

$$u_{k|k-1} = k_u u_{k-1} (0 < k_u < 1), \tag{25}$$

$$v_{k|k-1} = \frac{v_{k-1}}{u_{k-1} - 1} (u_{k|k-1} - 1), \tag{26}$$

and the measurement likelihood $g_k(h|a)$ obeys the gamma distribution, i.e.,

$$g_k(h|a) = G(h; \xi, \frac{\xi}{a}). \tag{27}$$

Thus, feature a is also an inverse gamma distribution after the prediction and update step:

$$f_{k|k}(a) \propto A_z(h) \cdot IG(a; u_{k|k}, v_{k|k}), \tag{28}$$

where

$$A_z(h) = \frac{v_{k|k-1}^{u_{k|k-1}}}{\Gamma(u_{k|k-1})} \frac{\xi^\xi}{\Gamma(\xi)} \frac{\Gamma(u_{k|k})}{v_{k|k}^{u_{k|k}}} h^{\xi-1}, \tag{29}$$

$$u_{k|k} = \xi + u_{k|k-1}, \tag{30}$$

$$v_{k|k} = v_{k|k-1} + \xi h. \tag{31}$$

The larger the parameter ξ is the greater the influence the measurement h has on the estimation.

Assume that the single-target kinematic states $\tilde{\mathbf{x}}$, the Markov transfer density $L_{k|k-1}(\tilde{\mathbf{x}}|\tilde{\mathbf{x}}')$ with state $\tilde{\mathbf{x}}'$, and the measurement likelihood function $\tilde{g}_k(\tilde{\mathbf{z}}|\tilde{\mathbf{x}})$ at time $k-1$ are all Gaussian,

$$f_{k-1|k-1}(\tilde{\mathbf{x}}) = N(\tilde{\mathbf{x}}; \mathbf{m}_{k-1}, \mathbf{P}_{k-1}), \tag{32}$$

$$L_{k|k-1}(\tilde{\mathbf{x}}|\tilde{\mathbf{x}}') = N(\tilde{\mathbf{x}}; \mathbf{F}_{k-1}\tilde{\mathbf{x}}', \mathbf{Q}_{k-1}), \tag{33}$$

$$\tilde{g}_k(\tilde{\mathbf{z}}|\tilde{\mathbf{x}}) = N(\tilde{\mathbf{z}}; \mathbf{H}_k\tilde{\mathbf{x}}, \mathbf{R}_k), \tag{34}$$

where $N(\cdot; \mathbf{m}, \mathbf{P})$ denotes a Gaussian density with mean \mathbf{m} and covariance \mathbf{P} . \mathbf{F}_{k-1} is the state transition matrix, \mathbf{Q}_{k-1} is the process noise covariance, \mathbf{H}_k is the observation matrix, and \mathbf{R}_k denotes the observation noise covariance. Then the form of the kinematic state $\tilde{\mathbf{x}}$ remains unchanged after the prediction and update step:

$$f_{k-1|k}(\tilde{\mathbf{x}}) = N(\tilde{\mathbf{x}}; \mathbf{m}_{k|k-1}, \mathbf{P}_{k|k-1}), \tag{35}$$

$$f_{k|k}(\tilde{\mathbf{x}}) \propto q_z(\tilde{\mathbf{z}}) \cdot N(\tilde{\mathbf{x}}; \mathbf{m}_k, \mathbf{P}_k), \tag{36}$$

where

$$\mathbf{m}_{k|k-1} = \mathbf{F}_{k-1}\mathbf{m}_{k-1}, \tag{37}$$

$$\mathbf{P}_{k|k-1} = \mathbf{F}_{k-1}\mathbf{P}_{k-1}\mathbf{F}_{k-1}^T + \mathbf{Q}_{k-1}, \tag{38}$$

$$q_z(\tilde{\mathbf{z}}) = N(\tilde{\mathbf{z}}; \mathbf{m}_{k|k-1}, \mathbf{R}_k + \mathbf{H}_k\mathbf{P}_{k|k-1}\mathbf{H}_k^T), \tag{39}$$

$$\mathbf{m}_k(\tilde{\mathbf{z}}) = \mathbf{m}_{k|k-1} + \mathbf{K}_k(\tilde{\mathbf{z}} - \mathbf{H}_k\mathbf{m}_{k|k-1}), \tag{40}$$

$$\mathbf{P}_k = \mathbf{P}_{k|k-1} - \mathbf{K}_k\mathbf{H}_k\mathbf{P}_{k|k-1}, \tag{41}$$

$$\mathbf{K}_k = \mathbf{P}_{k|k-1}\mathbf{H}_k[\mathbf{R}_k + \mathbf{H}_k\mathbf{P}_{k|k-1}\mathbf{H}_k^T]^{-1}. \tag{42}$$

3. Multisensor Filters Based on IGGM Model

The prior density and the likelihood function of the feature a obey the inverse gamma distribution and gamma distribution, respectively, which are a pair of conjugate distributions. Thus, we can derive the analytical forms of the MS-CPHD/MeMber filters which estimate the detection probability based on the IGGM model.

3.1. The IGGM-MS-CPHD Filter

3.1.1. Prediction

Assume that at time $k-1$ the posterior PHD has the IGGM form

$$D_{k-1|k-1}(\mathbf{x}) = \sum_{i=1}^{J_{k-1|k-1}} w_{k-1|k-1}^{(i)} N(\tilde{\mathbf{x}}; \mathbf{m}_{k-1|k-1}^{(i)}, \mathbf{P}_{k-1|k-1}^{(i)}) IG(a; u_{k-1|k-1}^{(i)}, v_{k-1|k-1}^{(i)}). \tag{43}$$

The PHD of the birth RFS at time k is

$$D_{b,k}(\mathbf{x}) = \sum_{i=1}^{J_{b,k}} w_{b,k}^{(i)} N(\tilde{\mathbf{x}}; \mathbf{m}_{b,k}^{(i)}, \mathbf{P}_{b,k}^{(i)}) IG(a; u_{b,k}^{(i)}, v_{b,k}^{(i)}), \tag{44}$$

and the survival probability of the target with state \mathbf{x} is constant, i.e., $\rho_{sv}(\mathbf{x}) = \rho_{sv}$. $w_{k-1|k-1}^{(i)}$ and $w_{b,k}^{(i)}$ are the weights of the target state. $J_{k-1|k-1}$ and $J_{b,k}$ are component numbers. Then the predicted PHD also comprises IGGM with

$$D_{k|k-1}(\mathbf{x}) = \sum_{i=1}^{J_{k-1|k-1}} p_{sv} w_{k-1|k-1}^{(i)} N(\bar{\mathbf{x}}; \mathbf{m}_{k|k-1}^{(i)}, \mathbf{P}_{k|k-1}^{(i)}) IG(a; u_{k|k-1}^{(i)}, v_{k|k-1}^{(i)}) + \sum_{i=1}^{J_{b,k}} w_{b,k}^{(i)} N(\bar{\mathbf{x}}; \mathbf{m}_{b,k}^{(i)}, \mathbf{P}_{b,k}^{(i)}) IG(a; u_{b,k}^{(i)}, v_{b,k}^{(i)}) \tag{45}$$

where $u_{k|k-1}^{(i)}$, $v_{k|k-1}^{(i)}$, $\mathbf{m}_{k|k-1}^{(i)}$, and $\mathbf{P}_{k|k-1}^{(i)}$ are given in Equations (25), (26), (37), and (38).

3.1.2. Update

Suppose that at time k the predicted PHD of the multitarget is

$$D_{k|k-1}(\mathbf{x}) = \sum_{i=1}^{J_{k|k-1}} w_{k|k-1}^{(i)} N(\bar{\mathbf{x}}; \mathbf{m}_{k|k-1}^{(i)}, \mathbf{P}_{k|k-1}^{(i)}) IG(a; u_{k|k-1}^{(i)}, v_{k|k-1}^{(i)}), \tag{46}$$

where $J_{k|k-1} = J_{k-1|k-1} + J_{b,k}$. Then the form of the multitarget PHD remains unchanged after the update step:

$$D_{k|k}(\mathbf{x}) = \sum_{i=1}^{J_{k|k-1}} \alpha_0 \prod_{j=1}^s q_d^j(a) \bar{w}_{k|k-1}^{(i)} N(\bar{\mathbf{x}}; \mathbf{m}_{k|k-1}^{(i)}, \mathbf{P}_{k|k-1}^{(i)}) IG(a; u_{k|k-1}^{(i)}, v_{k|k-1}^{(i)}) + \sum_{\mathbf{P} \in \mathbf{Q}} \sum_{j=1}^{|\mathbf{P}|-1} \sum_{i=1}^{J_{k|k-1}} w_{k|k}^{(\mathbf{W}_{1:s}^j, i)} N(\bar{\mathbf{x}}; \mathbf{m}_{k|k}^{(\mathbf{W}_{1:s}^j, i)}, \mathbf{P}_{k|k}^{(\mathbf{W}_{1:s}^j, i)}) IG(a; u_{k|k}^{(\mathbf{W}_{1:s}^j, i)}, v_{k|k}^{(\mathbf{W}_{1:s}^j, i)}) \tag{47}$$

where the updated weight is

$$w_{k|k}^{(\mathbf{W}_{1:s}^j, i)} = \bar{w}_{k|k-1}^{(i)} \prod_{(u,l) \in T_{\mathbf{W}_{1:s}^j}} p_d^u(a) q_z(\bar{\mathbf{z}}_l^u) A_z(h_l^u) \prod_{(v,*) \notin T_{\mathbf{W}_{1:s}^j}} q_v^v(a). \tag{48}$$

$\bar{w}_{k|k-1}^{(i)} = w_{k|k-1}^{(i)} / \sum_{j=1}^{J_{k|k-1}} w_{k|k-1}^{(j)}$ gives the normalized weight. The updated Gaussian function and inverse gamma function are determined by Equations (49) and (50):

$$N(\bar{\mathbf{x}}; \mathbf{m}_{k|k}^{(\mathbf{W}_{1:s}^j, i)}, \mathbf{P}_{k|k}^{(\mathbf{W}_{1:s}^j, i)}) \propto N(\bar{\mathbf{x}}; \mathbf{m}_{k|k-1}^{(i)}, \mathbf{P}_{k|k-1}^{(i)}) \prod_{(u,l) \in T_{\mathbf{W}_{1:s}^j}} \bar{g}_u(\bar{\mathbf{z}}_l^u | \bar{\mathbf{x}}), \tag{49}$$

$$IG(a; u_{k|k}^{(\mathbf{W}_{1:s}^j, i)}, v_{k|k}^{(\mathbf{W}_{1:s}^j, i)}) \propto IG(a; u_{k|k-1}^{(i)}, v_{k|k-1}^{(i)}) \prod_{(u,l) \in T_{\mathbf{W}_{1:s}^j}} g_u(h_l^u | a). \tag{50}$$

Moreover, the updated cardinality is given in Equation (10) with

$$\gamma = \sum_{n=1}^{J_{k|k-1}} \bar{w}_{k|k-1}^{(n)} \prod_{j=1}^s (1 - p_d^j(a_{k|k-1}^{(n)})), \tag{51}$$

$$d_{\mathbf{W}_{1:s}^j} = \frac{\left(\sum_{n=1}^{J_{k|k-1}} w_{k|k-1}^{(n)} \prod_{(i,l) \in T_{\mathbf{W}_{1:s}^j}} p_d^i(a_{k|k-1}^{(n)}) q_z(\bar{\mathbf{z}}_l^i) \times A_z(h_l^i) \prod_{(i,*) \notin T_{\mathbf{W}_{1:s}^j}} q_d^i(a_{k|k-1}^{(n)}) \right)}{\prod_{(i,l) \in T_{\mathbf{W}_{1:s}^j}} \bar{c}(\bar{\mathbf{z}}_l^i) A_z(h_l^i)}, \tag{52}$$

where, in Equations (51) and (52), the predicted feature a is estimated by the mean value, i.e., $a_{k|k-1}^{(n)} = v_{k|k-1}^{(n)} / (u_{k|k-1}^{(n)} - 1)$. $\tilde{c}(\cdot)$ is the spatial density function of the clutter.

3.2. The IGGM-MS-MeMber Filter

3.2.1. Prediction

Assume that at time $k-1$ the multitarget posterior has an IGGM form with $J_{k-1|k-1}^{(i)}$ components:

$$p_{k-1|k-1}^{(i)}(\mathbf{x}) = \sum_{n=1}^{J_{k-1|k-1}^{(i)}} w_{n,k-1|k-1}^{(i)} N(\tilde{\mathbf{x}}; \mathbf{m}_{n,k-1|k-1}^{(i)}, \mathbf{P}_{n,k-1|k-1}^{(i)}) IG(a; u_{n,k-1|k-1}^{(i)}, v_{n,k-1|k-1}^{(i)}). \tag{53}$$

The survival probability of the target $\rho_{sv,k}(\mathbf{x}) = \rho_{sv,k}$ is constant, and the density function of the newborn target is

$$p_{b,k}^{(i)}(\mathbf{x}) = \sum_{n=1}^{J_{b,k}^{(i)}} w_{b,n,k}^{(i)} N(\tilde{\mathbf{x}}; \mathbf{m}_{b,n,k}^{(i)}, \mathbf{P}_{b,n,k}^{(i)}) IG(a; u_{b,n,k}^{(i)}, v_{b,n,k}^{(i)}), \tag{54}$$

where $w_{n,k-1|k-1}^{(i)}$ and $w_{b,n,k}^{(i)}$ are the weights of the target state. Then the predicted density of each Bernoulli component also has the IGGM form, which can be obtained from Equations (13), (14), (53), and (54):

$$r_{S,k|k-1}^{(i)} = r_{k-1|k-1}^{(i)} \rho_{sv}, \tag{55}$$

$$p_{S,k|k-1}^{(i)}(\mathbf{x}) = \sum_{n=1}^{J_{k-1|k-1}^{(i)}} w_{n,k-1|k-1}^{(i)} N(\tilde{\mathbf{x}}; \mathbf{m}_{n,k|k-1}^{(i)}, \mathbf{P}_{n,k|k-1}^{(i)}) IG(a; u_{n,k|k-1}^{(i)}, v_{n,k|k-1}^{(i)}), \tag{56}$$

where $\mathbf{m}_{n,k|k-1}^{(i)}$, $\mathbf{P}_{n,k|k-1}^{(i)}$, $u_{n,k|k-1}^{(i)}$, and $v_{n,k|k-1}^{(i)}$ are respectively shown in Equations (25), (26), (37), and (38).

3.2.2. Update

Suppose that at time k the predicted density of each Bernoulli component is

$$p_{k|k-1}^{(i)}(\mathbf{x}) = \sum_{n=1}^{J_{k|k-1}^{(i)}} w_{n,k|k-1}^{(i)} N(\tilde{\mathbf{x}}; \mathbf{m}_{n,k|k-1}^{(i)}, \mathbf{P}_{n,k|k-1}^{(i)}) IG(a; u_{n,k|k-1}^{(i)}, v_{n,k|k-1}^{(i)}), \tag{57}$$

where $J_{k|k-1}^{(i)} = J_{k-1|k-1}^{(i)} + J_{b,k}^{(i)}$. Then this IGGM form remains unchanged after the update step, with

$$p_{k|k}^{(\mathbf{P},i)}(\mathbf{x}) = \sum_{n=1}^{J_{k|k-1}^{(i)}} w_{n,k|k}^{(\mathbf{P},i)} N(\tilde{\mathbf{x}}; \mathbf{m}_{n,k|k}^{(\mathbf{P},i)}, \mathbf{P}_{n,k|k}^{(\mathbf{P},i)}) IG(a; u_{n,k|k}^{(\mathbf{P},i)}, v_{n,k|k}^{(\mathbf{P},i)}), \tag{58}$$

$$r_{k|k}^{(\mathbf{P},i)} = \begin{cases} \alpha_{\mathbf{P}} \frac{r_{k|k-1}^{(i)} \sum_{n=1}^{J_{k|k-1}^{(i)}} \gamma(a_{n,k|k-1}^{(i)}) w_{n,k|k-1}^{(i)}}{1 - r_{k|k-1}^{(i)} + r_{k|k-1}^{(i)} \sum_{n=1}^{J_{k|k-1}^{(i)}} \gamma(a_{n,k|k-1}^{(i)}) w_{n,k|k-1}^{(i)}} & \mathbf{W}_{1:s}^i = \emptyset \\ \alpha_{\mathbf{P}} & \mathbf{W}_{1:s}^i \neq \emptyset \end{cases}, \tag{59}$$

where the Gaussian component, the inverse gamma component, and the updated weight after the update process are given as follows:

$$N(\bar{\mathbf{x}}; \mathbf{m}_{n,k}^{(P,i)}, \mathbf{P}_{n,k}^{(P,i)}) \propto \begin{cases} N(\bar{\mathbf{x}}; \mathbf{m}_{n,k|k-1}^{(i)}, \mathbf{P}_{n,k|k-1}^{(i)}) & \mathbf{W}_{1:s}^i = \emptyset \\ N(\bar{\mathbf{x}}; \mathbf{m}_{n,k|k-1}^{(i)}, \mathbf{P}_{n,k|k-1}^{(i)}) \prod_{(j,l) \in T_{\mathbf{W}_{1:s}^i}} \bar{g}_{j,k}(\bar{\mathbf{z}}_l^j | \bar{\mathbf{x}}) & \mathbf{W}_{1:s}^i \neq \emptyset \end{cases}, \quad (60)$$

$$IG(a; u_{n,k}^{(P,i)}, v_{n,k}^{(P,i)}) \propto \begin{cases} IG(a; u_{n,k|k-1}^{(i)}, v_{n,k|k-1}^{(i)}) & \mathbf{W}_{1:s}^i = \emptyset \\ IG(a; u_{n,k|k-1}^{(i)}, v_{n,k|k-1}^{(i)}) \prod_{(j,l) \in T_{\mathbf{W}_{1:s}^i}} g_{j,k}(h_l^j | a) & \mathbf{W}_{1:s}^i \neq \emptyset \end{cases}, \quad (61)$$

$$w_{n,k|k}^{(P,i)} \triangleq \begin{cases} \frac{\gamma(a_{n,k|k-1}^{(i)}) w_{n,k|k-1}^{(i)}}{\sum_{m=1}^{J_{k|k-1}^{(i)}} \gamma(a_{n,k|k-1}^{(i)}) w_{m,k|k-1}^{(i)}} & \mathbf{W}_{1:s}^i = \emptyset \\ \left(\frac{w_{n,k|k-1}^{(i)} \prod_{(j,l) \in T_{\mathbf{W}_{1:s}^i}} \frac{p_d^j(a_{n,k|k-1}^{(i)}) q_z(\bar{\mathbf{z}}_l^j) A_z(h_l^j)}{c(\mathbf{z}_l^j)}}{\prod_{(j,*) \notin T_{\mathbf{W}_{1:s}^i}} (1 - p_d^j(a_{n,k|k-1}^{(i)}))} \right) & \mathbf{W}_{1:s}^i \neq \emptyset \end{cases}. \quad (62)$$

$a_{n,k|k-1}^{(i)} = u_{n,k|k-1}^{(i)} / (v_{n,k|k-1}^{(i)} - 1)$ is the mean value of the feature a , and the clutter density function is $c(\mathbf{z}) = \bar{c}(\bar{\mathbf{z}}) \cdot A_z(h)$. The detection probability of sensor j is determined by

$$p_d^j(a) = \begin{cases} \varepsilon_1 \cdot (\exp((a - F_{th}) / \delta_1) - \varepsilon_2) & a < F_{th} \\ \varepsilon_1 \cdot (2 - \exp(-(a - F_{th}) / \delta_2) - \varepsilon_2) & a \geq F_{th} \end{cases}, \quad (63)$$

where F_{th} is the gate, $\varepsilon_1 = (2 - \exp(-F_{th} / \delta_1))^{-1}$, and $\varepsilon_2 = \exp(-F_{th} / \delta_1)$.

4. Simulation Results and Analysis

In this section, we explain the two simulation experiments we carried out to verify the proposed IGGM-MS-CPHD/MeMber filters. First, the proposed filters were compared with the GM-MS-CPHD/MeMber filters. Then, we analyzed the performance of the proposed algorithms under different sensor distributions. The optimal subpattern assignment (OSPA) distance [34] was used as the error metric:

$$d_p^{(c)}(\mathbf{X}, \mathbf{Y}) = \left(\frac{1}{n} \left(\min_{\pi \in \Pi_n} \sum_{i=1}^m \bar{d}^{(c)}(\mathbf{X}^{(i)}, \mathbf{Y}^{\pi(i)})^p + c^p(n - m) \right) \right)^{1/p}, \quad (64)$$

where order $p = 1$ and truncation threshold $c = 100$. $\mathbf{X} = \{x_1, \dots, x_m\}$ and $\mathbf{Y} = \{y_1, \dots, y_n\}$. $\bar{d}^{(c)}(x, y) = \min(d(x, y), c)$ denote the distance between vector x and y cutting off at threshold c . Π_n is the set of permutations on $\{1, 2, \dots, n\}$.

4.1. System Model

Figure 1 shows a two-dimensional scene with six targets in a uniform linear motion. Figure 2 shows the detection probability of targets and their detection feature a . In this paper, the amplitude of the target echo signal was taken as the detection feature. Each feature obeyed the sinusoidal distribution with a period of 40 s. The observation process lasted for 100 frames and the sampling period was $\Delta t = 1$ s.

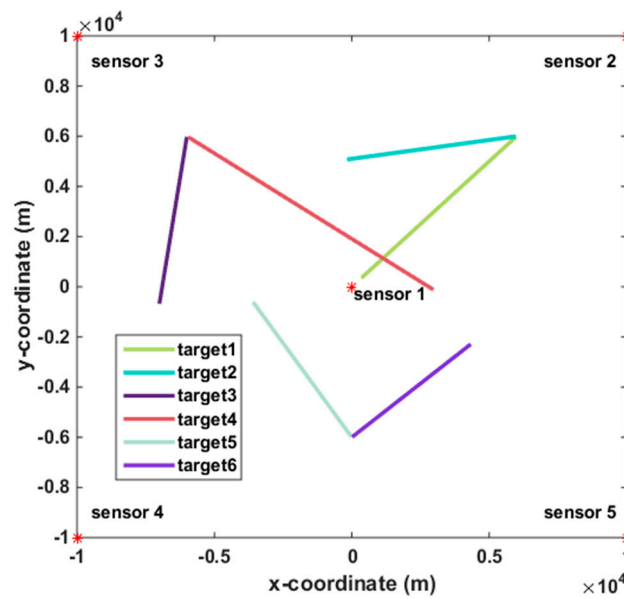


Figure 1. Truth trajectories of the target.

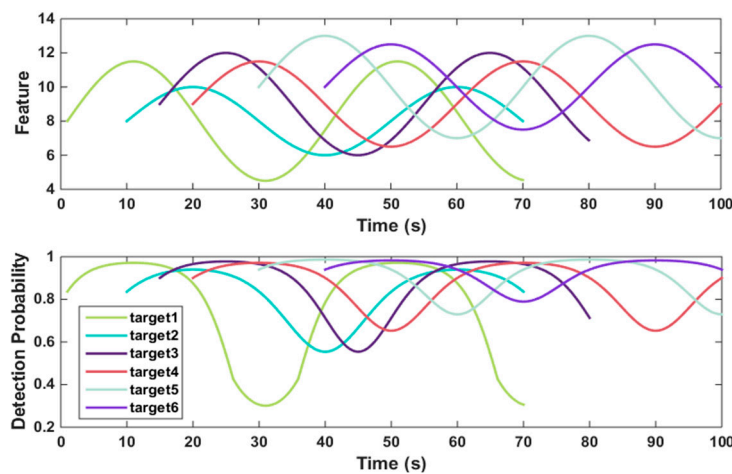


Figure 2. Target detection probability and the feature a .

The target state \mathbf{x} contains the kinematics state $\tilde{\mathbf{x}}$ and the detection feature a , where $\tilde{\mathbf{x}}_k = [p_{x,k}, \dot{p}_{x,k}, p_{y,k}, \dot{p}_{y,k}]^T$ denotes the position and velocity. The measurement \mathbf{z} also consists of the position measurement $\tilde{\mathbf{z}}$ and the feature measurement h , i.e., $\mathbf{z} = [\tilde{\mathbf{z}}, h]^T$, and $\tilde{\mathbf{z}} = [r_k, \theta_k]^T$ is the range and bearing information. In Equation (33), the state transition matrix and the process noise covariance matrix are respectively

$$F_{k-1} = \begin{bmatrix} 1 & \Delta t & 0 & 0 \\ 0 & 1 & 0 & 0 \\ 0 & 0 & 1 & \Delta t \\ 0 & 0 & 0 & 1 \end{bmatrix} Q_{k-1} = \begin{bmatrix} \frac{\Delta t^3}{3} & \frac{\Delta t^2}{2} & 0 & 0 \\ \frac{\Delta t^2}{2} & \Delta t & 0 & 0 \\ 0 & 0 & \frac{\Delta t^3}{3} & \frac{\Delta t^2}{2} \\ 0 & 0 & \frac{\Delta t^2}{2} & \Delta t \end{bmatrix} \sigma_v^2, \tag{65}$$

where the standard deviation of the process noise is $\sigma_v = 8 \text{ m/s}^2$.

For the nonlinear observation model, the extended Kalman filter (EKF) method [35] was used. The observation matrix and the measurement noise covariance matrix of sensor i are given as follows:

$$H_k^i = \begin{bmatrix} \frac{\tilde{p}_{x,k|k-1}}{\sqrt{\tilde{p}_{x,k|k-1}^2 + \tilde{p}_{y,k|k-1}^2}} & 0 & \frac{\tilde{p}_{y,k|k-1}}{\sqrt{\tilde{p}_{x,k|k-1}^2 + \tilde{p}_{y,k|k-1}^2}} & 0 \\ -\frac{\tilde{p}_{y,k|k-1}}{\tilde{p}_{x,k|k-1}^2 + \tilde{p}_{y,k|k-1}^2} & 0 & \frac{\tilde{p}_{x,k|k-1}}{\tilde{p}_{x,k|k-1}^2 + \tilde{p}_{y,k|k-1}^2} & 0 \end{bmatrix}, R_k = \begin{bmatrix} \sigma_r^2 & 0 \\ 0 & \sigma_\theta^2 \end{bmatrix}. \tag{66}$$

The measurement noise in range and bearing are $\sigma_r = 30$ m and $\sigma_\theta = 1^\circ$, respectively. $\tilde{p}_{x,k|k-1} = p_{x,k|k-1} + \tau_x^i$ and $\tilde{p}_{y,k|k-1} = p_{y,k|k-1} + \tau_y^i$, where $[\tau_x^i, \tau_y^i]^T$ is the coordinate offset of the sensor i with respect to the fusion center.

In the simulation, the target survival probability $\rho_{sv,k}$ was set to 0.99. As shown in Table 1, the birth model was set according to the target initial states. For the detection feature a in the prediction process, we set the transfer parameter k_u to 0.7, and the parameter in measurement likelihood was set to $\xi = 3$. In Equation (63), we set F_{th} to 5.5, δ_1 to 4, and δ_2 to 2. We assumed that the clutter measurements generated by the sensors were Poisson with the uniform spatial distribution $\tilde{c}(\tilde{\mathbf{z}})$ and mean clutter rate λ_c , i.e., $\kappa_k(\mathbf{z}) = \lambda_c \tilde{c}(\tilde{\mathbf{z}}) \int IG(a; u_k^\kappa, v_k^\kappa) \cdot g_k(h|a) da$.

Table 1. The target initial states.

| Target | State $\tilde{\mathbf{x}}$ | u | v | Survival Time (s) |
|--------|------------------------------|-----|-----|-------------------|
| 1 | $[6000, -80, 6000, -80]^T$ | 51 | 400 | [1 70] |
| 2 | $[6000, -100, 6000, -15]^T$ | 51 | 400 | [10 70] |
| 3 | $[-6000, -15, 6000, -100]^T$ | 41 | 360 | [15 80] |
| 4 | $[-6000, 110, 6000, -75]^T$ | 41 | 360 | [20 100] |
| 5 | $[0, -50, -6000, 75]^T$ | 51 | 500 | [30 100] |
| 6 | $[0, 70, -6000, 60]^T$ | 51 | 500 | [40 100] |

For efficiency purposes, the pruning and merging methods in [10,29] were adopted in this paper. For the greedy measurement partitioning algorithm, the maximum number of the measurement subsets W_{max} was set to 4, and the maximum number of partitioning hypotheses P_{max} was set to 4. In the GM-MS-CPHD/MeMber filters, the detection probability p_d was fixed at 0.9.

4.2. Simulation 1

This section verifies the performance of the proposed IGGM-MS-CPHD/MeMber filters in scenarios where the detection probability is unknown and dynamically changing. As shown in Figure 1, the sensors were located at [0 km, 0 km], [10 km, 10 km], [-10 km, 10 km], [-10 km, -10 km], and [10 km, -10 km], respectively. We took Sensor 1 as the fusion center, and the scopes of the sensors are shown in Table 2.

Table 2. The scopes of the sensors.

| Sensor | Range r | Bearing θ |
|--------|-----------|------------------|
| 1 | 0–10 km | 0–360° |
| 2 | 0–25 km | 180–270° |
| 3 | 0–25 km | 270–360° |
| 4 | 0–25 km | 0–90° |
| 5 | 0–25 km | 90–180° |

The average clutter intensity λ_c was set to 10, with shape parameter u_k^κ set to 31 and scale parameter v_k^κ set to 280. Figure 3 shows the observation results of the sensors, in which the black dots represent the measurements.

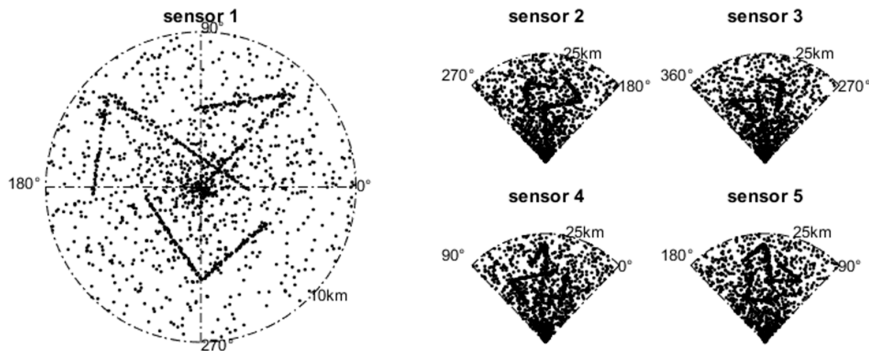


Figure 3. Measurement of the sensors.

Specifically, we compared the traditional GM-MS-CPHD/MeMber filters with the IGGM-MS-CPHD/MeMber filters derived in this paper. The average OSPA and the cardinality estimation of the four algorithms with 100 Monte Carlo runs are shown in Figures 4 and 5. It can be seen that at the beginning of the filtering process the four filters achieve similar filtering performance. The detection probability of Target 1 was lower than 0.4 at about 30 s, while the parameter was fixed at $pd = 0.9$. As the detection probability decreases the filtering performance of the GM-MS-CPHD/MeMber filters begins to deteriorate with a cardinality estimation bias. In contrast, the proposed IGGM-MS-CPHD/MeMber filters have lower OSPA distances and obtain a smaller deviation of the estimated cardinality.

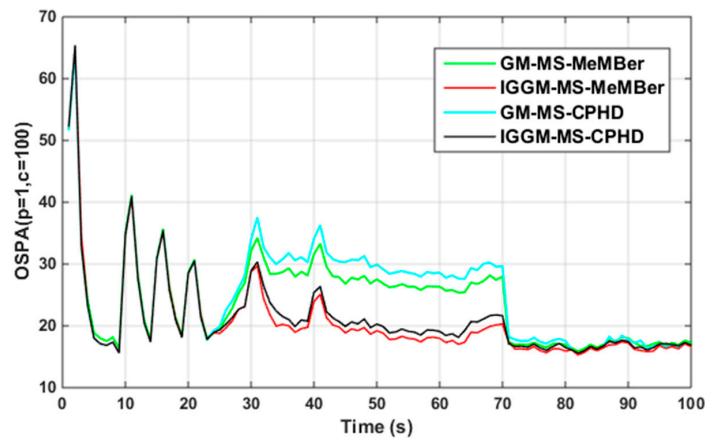


Figure 4. Optimal subpattern assignment (OSPA) distance.

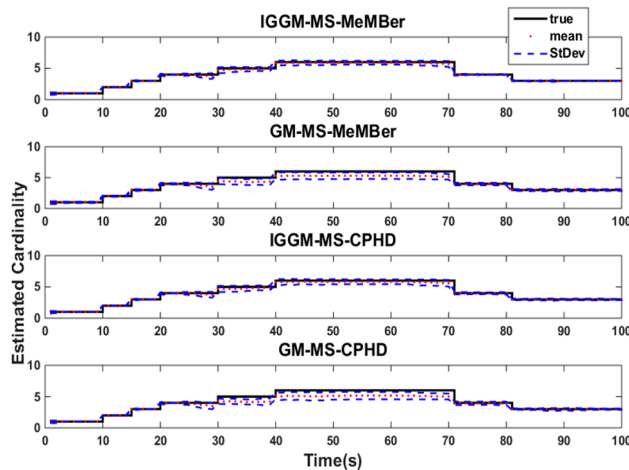


Figure 5. Estimation of the cardinality.

Table 3 shows the average single-step running time of the four algorithms with 100 Monte Carlo simulations. It can be seen that the proposed IGGM-MS-CPHD/MeMber filters have a higher computational cost, and the IGGM-MS-CPHD filter demands the longest time.

Table 3. Average single-step running time.

| IGGM-MS-CPHD | IGGM-MS-MeMber | GM-MS-CPHD | GM-MS-MeMber |
|--------------|----------------|------------|--------------|
| 180 ms | 75 ms | 127 ms | 58 ms |

The filtering performances under different clutter intensities are shown in Figures 6 and 7. We observed that a higher clutter intensity leads to a larger OSPA distance and more computational cost. By comparison, the IGGM-MS-MeMber filter is the most efficient method.

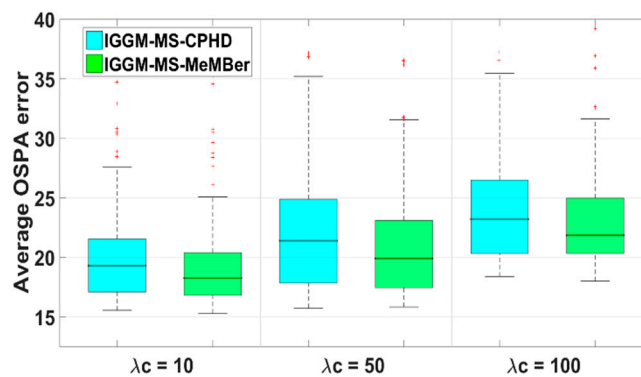


Figure 6. OSPA distances for different clutter intensities.

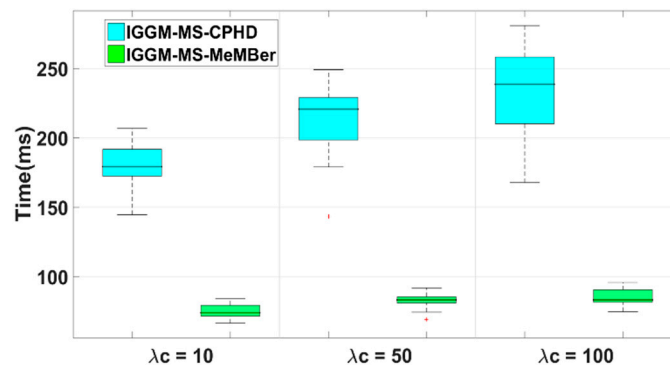


Figure 7. Average running times for different clutter intensities.

4.3. Simulation 2

This section analyzes the performance of IGGM-MS-CPHD/MeMber filters under different sensor distributions. Suppose that there are four sensors in the two-dimensional space for observation. All sensors have the same scope with bearing $\theta \in (0-360^\circ)$ and range $r \in (0-25 \text{ km})$, and the other parameters are the same as those in Simulation 1. Three distributions of sensors are given as follows:

- Case 1: assume that the four sensors are located at $[-10 \text{ km}, 10 \text{ km}]$, $[-10 \text{ km}, -10 \text{ km}]$, $[10 \text{ km}, -10 \text{ km}]$, and $[10 \text{ km}, 10 \text{ km}]$, respectively;
- Case 2: assume that the four sensors are located at $[-10 \text{ km}, 0 \text{ km}]$, $[0 \text{ km}, -10 \text{ km}]$, $[10 \text{ km}, 0 \text{ km}]$, and $[0 \text{ km}, 10 \text{ km}]$, respectively;
- Case 3: assume that the four sensors are located at $[-9 \text{ km}, -10 \text{ km}]$, $[-3 \text{ km}, -10 \text{ km}]$, $[3 \text{ km}, -10 \text{ km}]$, and $[9 \text{ km}, -10 \text{ km}]$, respectively.

The performance of IGGM-MS-CPHD/MeMber filters under different sensor distributions is shown in Figure 8. It can be seen that the distribution of sensors has an important effect on the filtering errors, while the running time is barely affected by the sensor distributions. We observed that the proposed IGGM-MS-CPHD/MeMber filters and the GM-MS-CPHD/MeMber filters can achieve a better filtering accuracy when the sensors are dispersed in the monitoring area (e.g., Cases 1 and 2).

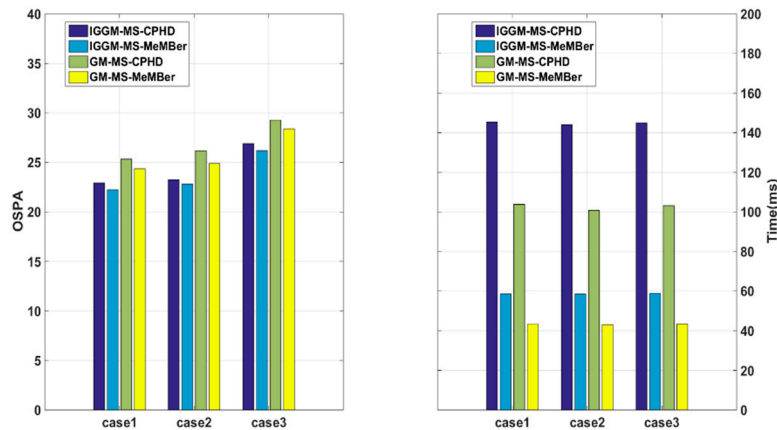


Figure 8. Performance under different sensor distributions.

5. Conclusions

In this paper, a multisensor CPHD filter and a multisensor MeMber filter were derived for the unknown and varying detection probability case. By using the IGGM model, the proposed filters can estimate the unknown and changing detection probability. The simulation results show that the proposed methods have improved filtering performances as well as higher computational costs with unknown and dynamically changing detection probability. We also conclude that the distribution of sensors has an important influence on the filtering accuracy, and the filters perform better when the sensors are dispersed in the monitoring area. Future work will explore the multisensor multitarget filter, which can estimate the clutter intensity and the detection probability adaptively, and refine the proposed algorithms in this paper to output target tracks.

Author Contributions: Z.Z. and J.S. conceived the idea, Z.Z. and Q.L. conducted the experiments and wrote the initial draft of the paper, and J.S. and Q.L. revised the manuscript. All authors read and approved the manuscript.

Funding: This work was supported by the National Natural Science Foundation of China (61471019).

Conflicts of Interest: The authors declare no conflict of interest.

References

- Mahler, R.P.S. *Advances in Statistical Multisource-Multitarget Information Fusion*; Artech House: Norwood, MA, USA, 2014.
- Quan, H.W.; Li, J.H.; Peng, D.L. Multi-target Tracking Based on Random Set Theory. *Fire Control Command Control* **2015**, *40*, 49–56.
- Shen, T.H.; Xue, A.K.; Zhou, Z.L. Multi-sensor Gaussian Mixture PHD Fusion for Multi-target Tracking. *Acta Autom. Sin.* **2017**, *43*, 1028–1037.
- Reid, D. An algorithm for tracking multiple targets. *IEEE Trans. Autom. Control* **1979**, *24*, 843–854. [[CrossRef](#)]
- Kirubarajan, T.; Bar-Shalom, Y. Probabilistic data association techniques for target tracking in clutter. *Proc. IEEE* **2004**, *92*, 536–557. [[CrossRef](#)]
- Mahler, R.P.S. *Statistical Multisource-Multitarget Information Fusion*; Artech House: Norwood, MA, USA, 2007.
- Vo, B.N.; Ma, W.K. The Gaussian Mixture Probability Hypothesis Density Filter. *IEEE Trans. Signal Process.* **2006**, *54*, 4091–4104. [[CrossRef](#)]
- Vo, B.T.; Vo, B.N.; Cantoni, A. Analytic Implementations of the Cardinalized Probability Hypothesis Density Filter. *IEEE Trans. Signal Process.* **2007**, *55*, 3553–3567. [[CrossRef](#)]

9. Vo, B.T.; Vo, B.N.; Cantoni, A. On multi-Bernoulli approximations to the Bayes multi-target filter. In Proceedings of the International Colloquium on Information Fusion, Xi'an, China, 22–25 August 2007.
10. Vo, B.T.; Vo, B.N.; Cantoni, A. The Cardinality Balanced Multi-Target Multi-Bernoulli Filter and Its Implementations. *IEEE Trans. Signal Process.* **2009**, *57*, 409–423.
11. Vo, B.T.; Vo, B.N. Labeled random finite sets and multi-object conjugate priors. *IEEE Trans. Signal Process.* **2013**, *61*, 3460–3475. [[CrossRef](#)]
12. Reuter, S.; Vo, B.T.; Vo, B.N.; Dietmayer, K. The labeled multi-Bernoulli filter. *IEEE Trans. Signal Process.* **2014**, *62*, 3246–3260.
13. Fantacci, C.; Vo, B.T.; Papi, F.; Vo, B.N. The Marginalized delta-GLMB Filter. *arXiv* **2015**, arXiv:1501.00926.
14. Mertens, M.; Ulmke, M. Ground moving target tracking using signal strength measurements with the GM-CPHD filter. In Proceedings of the 2012 Workshop on Sensor Data Fusion: Trends, Solutions, Applications (SDF), Bonn, Germany, 4–6 September 2012.
15. Maggio, E.; Taj, M.; Cavallaro, A. Efficient Multitarget Visual Tracking Using Random Finite Sets. *IEEE Trans. Circuits Syst. Video Technol.* **2008**, *18*, 1016–1027. [[CrossRef](#)]
16. Kim, D.Y.; Jeon, M. Robust multi-Bernoulli filtering for visual tracking. In Proceedings of the International Conference on Control, Automation and Information Sciences (ICCAIS 2014), Gwangju, Korea, 2–5 December 2014; pp. 47–51.
17. Mahler, R.P.S. The multisensor PHD filter: I. General solution via multitarget calculus. *Proc. Spie Int. Soc. Opt. Eng.* **2009**, 7336.
18. Delande, E.; Duflos, E.; Heurguier, D.; Vanheeghe, P. *Multi-Target PHD Filtering: Proposition of Extensions to the Multi-Sensor Case*; Research Report RR-7337; HAL-INRIA: Le Chesnay, French, 2010; p. 64.
19. Mahler, R.P.S. The multisensor PHD filter: II. Erroneous solution via Poisson magic. In Proceedings of the SPIE International Conference on Signal Processing, Sensor Fusion, Target Recognition, Orlando, FL, USA, 13–17 April 2009.
20. Mahler, R.P.S. Approximate multisensor CPHD and PHD filters. In Proceedings of the International Conference on Information Fusion, Edinburgh, UK, 26–29 July 2010.
21. Nannuru, S.; Blouin, S.; Coates, M.; Rabbat, M. Multisensor CPHD filter. *IEEE Trans. Aerosp. Electron. Syst.* **2016**, *52*, 1834–1854. [[CrossRef](#)]
22. Saucan, A.A.; Coates, M.J.; Rabbat, M. A Multisensor Multi-Bernoulli Filter. *IEEE Trans. Signal Process.* **2017**, *65*, 5495–5509. [[CrossRef](#)]
23. Wei, B.; Nener, B.; Liu, W.; Ma, L. Centralized multi-sensor multi-target tracking with labeled random finite sets. In Proceedings of the International Conference on Control, Automation and Information Sciences (ICCAIS), Ansan, Korea, 27–29 October 2016.
24. Ren, X.Y. *A Novel Multiple Target Tracking Algorithm and Its Evaluation*; Graduate University of Chinese Academy of Sciences: Beijing, China, May 2012.
25. Mahler, R.P.S.; Vo, B.T.; Vo, B.N. CPHD filtering with unknown clutter rate and detection profile. *IEEE Trans. Signal Process.* **2011**, *59*, 3497–3513. [[CrossRef](#)]
26. Vo, B.T.; Vo, B.N.; Hoseinnezhad, R.; Mahler, R.P.S. Multi-Bernoulli filtering with unknown clutter intensity and sensor field-of-view. In Proceedings of the 45th Annual Conference on Information Sciences and Systems (CISS), Baltimore, MD, USA, 23–25 March 2011.
27. Vo, B.T.; Vo, B.N.; Hoseinnezhad, R.; Mahler, R.P.S. Robust Multi-Bernoulli filtering. *IEEE J. Sel. Top. Signal Process.* **2013**, *7*, 399–409. [[CrossRef](#)]
28. Punchihewa, Y.; Vo, B.T.; Vo, B.N.; Kim, D.Y. Multiple Object Tracking in Unknown Backgrounds with Labeled Random Finite Sets. *IEEE Trans. Signal Process.* **2017**, *66*, 3040–3055. [[CrossRef](#)]
29. Li, C.; Wang, W.; Kirubarajan, T.; Sun, J.; Lei, P. PHD and CPHD Filtering with Unknown Detection Probability. *IEEE Trans. Signal Process.* **2018**, *66*, 3784–3798. [[CrossRef](#)]
30. Qian, K.; Zhou, H.; Qin, H.; Rong, S.; Zhao, D.; Du, J. Guided filter and convolutional network based tracking for infrared dim moving target. *Infrared Phys. Technol.* **2017**, *85*, 431–442. [[CrossRef](#)]
31. Lerro, D.; Bar-Shalom, Y. Automated Tracking with Target Amplitude Information. In Proceedings of the American Control Conference, San Diego, CA, USA, 23–25 May 1990; pp. 2875–2880.
32. Clark, D.; Ristic, B.; Vo, B.N.; Vo, B.T. Bayesian Multi-Object Filtering With Amplitude Feature Likelihood for Unknown Object SNR. *IEEE Trans. Signal Process.* **2010**, *58*, 26–37. [[CrossRef](#)]
33. Skolnik, M. *Radar Handbook*, 3rd ed.; McGraw-Hill: New York, NY, USA, 2008.

34. Schuhmacher, D.; Vo, B.T.; Vo, B.N. A consistent metric for performance evaluation of multi-object filters. *IEEE Trans. Signal Process.* **2008**, *56*, 3447–3457. [[CrossRef](#)]
35. Grewal, M.S.; Andrews, A.P. *Kalman Filtering: Theory and Practice Using MATLAB*, 3rd ed.; Wiley: Hoboken, NJ, USA, 2008.



© 2019 by the authors. Licensee MDPI, Basel, Switzerland. This article is an open access article distributed under the terms and conditions of the Creative Commons Attribution (CC BY) license (<http://creativecommons.org/licenses/by/4.0/>).